Novel tuffite/Fe-Cu oxides nanocomposite with functionality for dye removal in aqueous solution

Alien Blanco-Flores[a,b,*], Victor Sánchez-Mendieta[b], Edith Gutiérrez-Segura[b], Alfredo R. Vilchis-Néstor[c], Raul A. Morales-Luckie[b]

[a] División de Mecánica, Tecnológico de Estudios Superiores de Tianguistenco, Carretera Tenango-Marquesa Km 22, Santiago Tilapa, C.P. 52650, Santiago Tianguistenco, Estado de México, Mexico
[b] Facultad de Química, Universidad Autónoma del Estado de México, Paseo Colón y Tollocan s/n., C.P. 50000 Toluca, Estado de México, Mexico
[c] Centro Conjunto de Investigación en Química Sustentable UAEM-UNAM, Carretera Toluca, Atlacomulco Km 14.5, Unidad San Cayetano, C.P. 50200, Toluca, Estado de México, Mexico

A B S T R A C T

Fe-Cu oxides nanoparticles were embedded on tuffite (TUF) mineral by means of a simple immersion-ion impregnation, followed by a reduction reaction, methodology. TUF/Fe-Cu nanocomposite characteristics were investigated by XRD, TEM, BET, SEM, FT-IR spectroscopy and pH_{zpc} method. Fe-Cu nanostructures with mean sizes between 10 and 20 nm were effectively supported on TUF. Because of its functional properties, the nanocomposite was studied as adsorbent material for the degradation of malachite green (MG) organic dye in aqueous solution. The adsorption kinetic data was well-fitted to pseudo first-order model, indicating physisorption as the main mechanism of adsorption. High pH and temperature of the solution favored malachite green adsorption. The adsorption process was spontaneous and endothermic. In comparative sorption experiments with different dyes, the nanocomposite showed better removal capacities for cationic and basic than for anionic and acid dyes. Langmuir, Freundlich, Langmuir-Freundlich and Temkin models were applied to evaluate the isotherms, resulting in an adsorption capacity of 376.66 mg/g, which is above most of the adsorbent materials so far employed for malachite green degradation in aqueous solution. Therefore, this novel, easy to prepare and low-cost nanocomposite proved to have synergic functionality as an efficient adsorbent material for cationic organic dyes.

© 2016 Elsevier Ltd. All rights reserved.

1. Introduction

The presence of many contaminants in surface water is a real worldwide problem, due to growth population and increase of industrial activities. In this sense, it is necessary to control the water pollution and negative effects of organic and inorganic contaminant [1]. This could be achieved through efficient wastewater treatments, which include the adsorption process. Implementation of adsorption process is generally cheap providing that adsorbent materials are low cost and abundant, like natural minerals such as: zeolites, tuffs and clays, among others [2].

Recently, nanoparticles have been suggested as efficient, cost-effective and environmental friendly alternative specifically metallic nanoparticles, which have relatively higher chemical activity and specificity of interaction [3]. In general, the nanoparticles work in two-fold ways: like adsorbent material and as reducing agent of organic compound, such as dyes. Among other characteristics, they have a high specific surface area. All these aspects could help to improve the technology of actual methods of wastewater treatment. However, these nanomaterials have a disadvantage related to the industrial application since usually they cannot be used by themselves. They can be injected directly into the effluent, however, their separation and recovery after the process is as difficult as expensive. This is the main reason why they should therefore be supported [4]. Researchers have proposed to support nanoparticles on porous, natural or synthetic, materials. This ensures that the separation process will be simple and more easily performed through a filtration operation [5]. Besides,

* Corresponding author at: División de Mecánica, Tecnológico de Estudios Superiores de Tianguistenco, Carretera Tenango-Marquesa Km 22, Santiago Tilapa, Santiago Tianguistenco 52650, Mexico.
E-mail address: blancoflores81@hotmail.com (A. Blanco-Flores).

researchers have found that an heterogeneous composite has better efficiency than single nanoparticles; in some cases they even develop new synergic properties. Natural materials that have been recently used as low cost effective supports for nanoscale are pillared clays and zeolites such as montmorillonite [6], clinoptilolite [7] and MCM-41 [8] or sewage sludge converted in carbonaceous material [9]. Another low cost adsorbent material is tuff, which is a mineral rich in calcium carbonate. $CaCO_3$ precipitation in tuff produces a vast array of crystal forms; calcite predominates in most instances, followed by aragonite, and to a lesser extent $MgCO_3$. The SiO_2 and MgO are the next most abundant compounds and minor levels of Al_2O_3 and Fe_2O_3 are also found [10]. These characteristics, which include their availability and abundance, make them low cost adsorbent materials that can be used as templates for nanoparticles.

It is well known that zero-valent iron and iron oxides are effective for organic dyes degradation and improves of biodegradability [11]. The addition of other transition metal, such as copper, may enhance the reactivity of nanoparticles and degradation rates of aquatic contaminants acting through the synergistic effect between bimetallic system and composite [12]. According to this idea, iron-copper oxides nanocomposites have been synthesized to enhance dyes removal [3,7,13,14], but the degradation of organic dyes using Fe-Cu nanocomposites remains a scarcely explored area.

Previously, we have studied that the combination between porous materials and metal nanoparticles is one of the most interesting areas of interdisciplinary research in water treatments [7]. The aims of our present study are to synthesize and characterize TUF/Fe-Cu 95/5 wt.% composite and to evaluate its sorption properties to remove organic dyes, particularly malachite green, from aqueous solution.

2. Experimental

2.1. Materials and reagents

The tufa (TUF) samples used in this work were collected from the east province Holguín in Cuba. TUF was ground and sieved with a 60 mesh (0.25 mm) particle size sieve. Malachite green chloride (MG), a basic dye, (CI = 42000, molecular formula: $C_{23}H_{25}N_2Cl$, pKa: 6.9 and molecular weight = 365 g/mol). Acid green 25 (AG), an acid dye, (CI = 61570, molecular formula: $C_{23}H_{18}C1N_4Na_2O_7S_2$, pKa: 6.5 and molecular weight = 622.58 g/mol) and congo red (CR) (CI = 22120, molecular formula: $C_{32}H_{22}N_6Na_2O_6S_2$, pKa: 5.5 and molecular weight = 696.7 g/mol) (Hycel, México) were used without further treatment. Dyes solutions were prepared by dissolving an appropriate amount of dye in distilled water to obtain a range of concentrations corresponding to 30–120 mg/L for successive dilutions.

2.2. Synthesis

TUF/Fe-Cu(95–5 wt.%) nanocomposite was obtained by impregnation-chemical reduction synthesis according to the method reported in the literature [13]. $FeSO_4 \cdot 7H_2O$ and $CuSO_4 \cdot 5H_2O$ (Fermont, México) were dissolved in distilled water and TUF was added to the reaction medium. The mixture was stirred at room temperature for a fixed contact time. Later the pH was adjusted (pH = 7) and $NaBH_4$ was added quickly into the mixture. Subsequently, it was filtrated and the composite was washed with distilled water followed by acetone. The product was dried in an oven at 40 °C and stored in a closed container until further use. After several trials, the best experimental conditions to obtain this composite were: a volume of bimetallic aqueous solution of 100 mL and a contact time of 60 min.

2.3. Characterization

The surface morphology analyses of the composite were performed by scanning electron microscope (SEM) using a JEOL JSM-6510LV SEM microscope operated at 20 kV. Samples were fixed on a support with a carbon film and sputter-coated with gold to a thickness of ~200 Å. Transmission electron microscopy (TEM) observations were carried out using a JEOL 2100 microscope operated at 200 kV accelerating voltage. For TEM observations, the composite was dispersed by ultrasound in 2-propanol at room temperature (25 °C). A drop of the suspension was then placed on a carbon-coated Cu grid. In order to obtain statistically consistent information on the particle size distribution, the length of about 200 particles was measured, employing ImageJ™ software. The composite phases analysis were investigated by X-ray powder diffraction (XRD) analysis. The XRD analysis was performed in a Bruker D8 Advance diffractometer with a Cu K_α radiation source operating at 30 kV and a tube current of 25 mA. XRD diagrams were acquired with values of 2θ from 5 to 80, with a step size of 0.03. The surface properties and surface area of the composite, were characterized by N_2 adsorption measurements at 77 K using a surface area analyzer (Micromeritics Gemini 2360 instrument). The BET specific surface areas were determined by standard multipoint techniques of nitrogen adsorption. The determination of pore size was carried out by the method of BJH according to implemented software routines. Fourier transform infrared (FT-IR) spectroscopy analyses were performed using a spectrometer Nicolet Magna IRTM 550 FTIR. The determination of pH_{zpc} of TUF/Fe-Cu nanocomposite was performed by applying the method reported on the literature [15], using a pH meter Conductronic pH 120.

2.4. Kinetic adsorption experiments

The influence of the contact time over an amount of organic dye removal by the TUF/Fe-Cu nanocomposite was studied through batch experiments, at a dye initial concentration of 50 mg/L, adding 10 mL of dye solution to 10 mg of nanocomposite. The mixture was shaken at different times at 120 rpm, and the adsorbent was separated by centrifugation and after decanted. The experiments were performed in duplicate.

To analyze the effect of dye structure three kind of dye were studied: basic dye (malachite green), acid dye (acid green 25) and azo dye (congo red). To study the effect of pH and temperature on MG adsorption process, the dye solutions pH were adjust from 2 to 12 using 0.1 M HCl and 0.1 M NaOH solutions and the temperature values were 293, 303 and 313 K respectively.

2.5. Adsorption isotherms

10 mg of TUF/Fe-Cu nanocomposite was put in contact with 10 mL at different initial concentration of dye (30–120 mg/L) stirring during equilibrium time at room temperature. The mixture was centrifuged and decanted. The malachite green dye concentrations in the solutions were determined using a UV/Vis Perking Elmer Lambda 10 ultraviolet–visible spectrophotometer to 620 nm as maximum wavelength. The pH of each solution was measured before and after the treatments. The kinetic and adsorption data of the adsorbed amount of dye at time, q_t (mg/g of adsorbent), were obtained by Eq. (1):

$$\frac{(C_o - C_t) \cdot V}{m} = q_t \tag{1}$$

Where, C_o (mg/L) is the initial dye concentration, C_t (mg/L) is the concentration of the solution at time t, V (L) is the volume of

treated solution, and m (g) is the mass of TUF/Fe-Cu nano-composite.

3. Results and discussion

3.1. Synthesis of TUF/Fe-Cu nanocomposite

The TUF/Fe-Cu nanocomposite was prepared by synthesizing Fe-Cu nanostructures *in-situ* in an aqueous solution containing a certain amount of TUF mineral. Thus, Fe^{2+} and Cu^{2+} are sorbed or attached in TUF mineral micrometric particles (contact time), then, the main chemical reaction proceeds through reduction of iron and copper ions with sodium borohydride, according to the following stoichiometric equation

$$4Fe^{2+} + 4Cu^{2+} + 3BH_4^- + 12H_2O \rightarrow 4Fe^0Cu^0 + 3B(OH)_4 + 24H^+$$
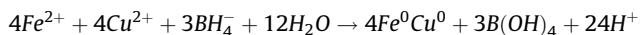
The physicochemical structure (pores, voids, chemical moieties) of TUF should work as nanoreactors, as have been demonstrated for several materials [5], where the nucleation, growth, coarsening, and some times agglomeration, processes of nanostructures occur. In addition, the presence of oxygen and stirring condition in the reaction allowed the zerovalent metals became mainly Fe and Cu oxides [16] and also, under the actual reaction conditions, to generate a Fe-Cu oxides nanoparticles [13].

3.2. TUF/Fe-Cu nanocomposite characterization

In Fig. 1 different diffraction patterns can be seen for TUF mineral and TUF/Fe-Cu nanocomposite, which are mainly the characteristic peaks related to the basic minerals found in TUF, calcite and clinoptilolite. Besides these peaks, there are others less intense peaks corresponding to iron oxides nanoparticles. Peaks found related to copper have the lowest intensity, this may have two explanations, the first one is because the amount of copper in the bymetallic system is very low, and the second one is associated to the plausible formation of a Fe-Cu oxide nanoparticles, in which it has already been studied by XRD that copper peaks usually do not appear [17].

TEM images of nanoparticles formed in the TUF/Fe-Cu nano-composite, and extracted as mentioned in the experimental section, are shown in Fig. 2. As can be observed, at least two different nanostructures shapes were found, some of the particles are spherical (a), connected in chain-like structure and other have
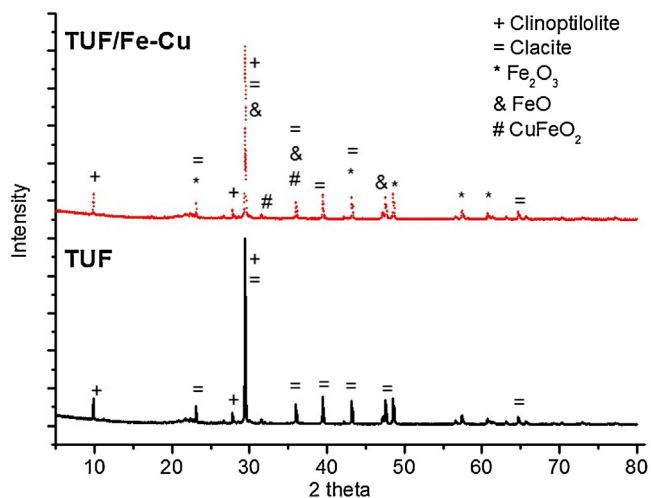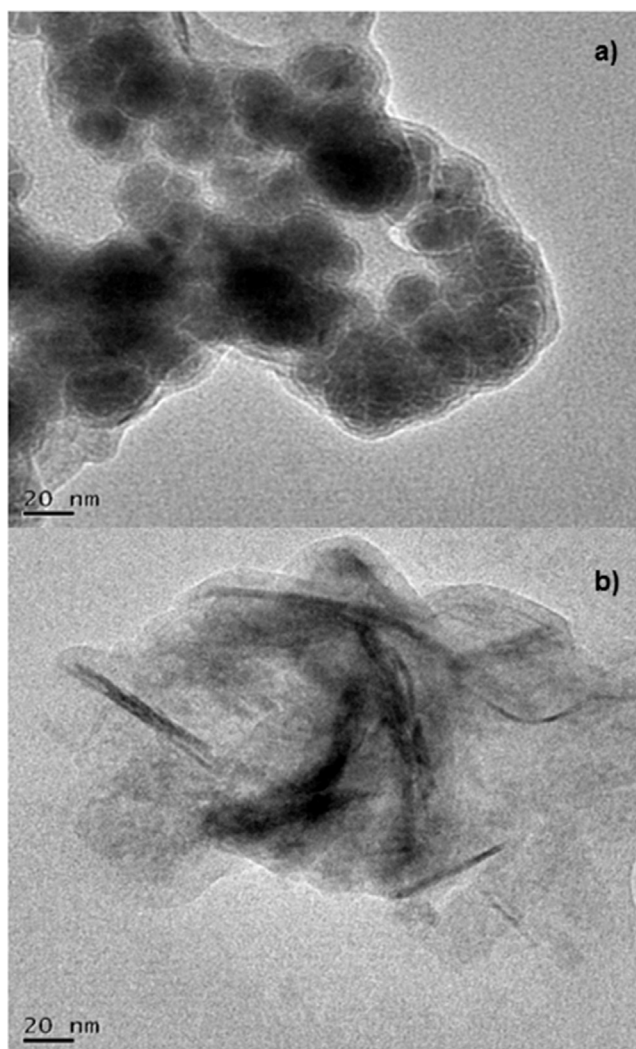

Fig. 2. TEM images of the Fe-Cu nanostructures formed in the TUF/Fe-Cu nanocomposite.

elongated form or needle-shape (b). Also, it can be noticed that the nanoparticles tend to form agglomerates.

The size of spherical nanoparticles oscillates between 10 and 20 nm (Fig. 3a). For needle-like nanoparticles the dispersion of size was higher, with an the average size of 15 nm of length (Fig. 3b). These results are consistent with those reported in works forming similar nanocomposites using different support materials [3,18]. These relatively small mean sizes of the thus obtained nano-particles can be associated to the fast way of adding to the mixture solution of the reducing agent ($NaBH_4$), which causes the rapid reduction rate of both metal ions to form nanoparticles fixed on TUF mineral.

The chemical composition of the TUF/Fe-Cu nanocomposite was obtained through mapping chemical and lineal profile of chemical composition from STEM analysis.

As observed in EDS maps, copper and iron moieties (Fig. 4) show similar distributions along the support material which can be associate to an homogenous distribution of the both nanoparticles on the mineral; although, iron nanostructures, accordingly to their higher concentration.

Lineal profile of chemical composition of the TUF/Fe-Cu nanocomposite (Fig. 5a and b) confirm the results obtained by TEM and EDS mapping. The intensity profiles of signals indicate the
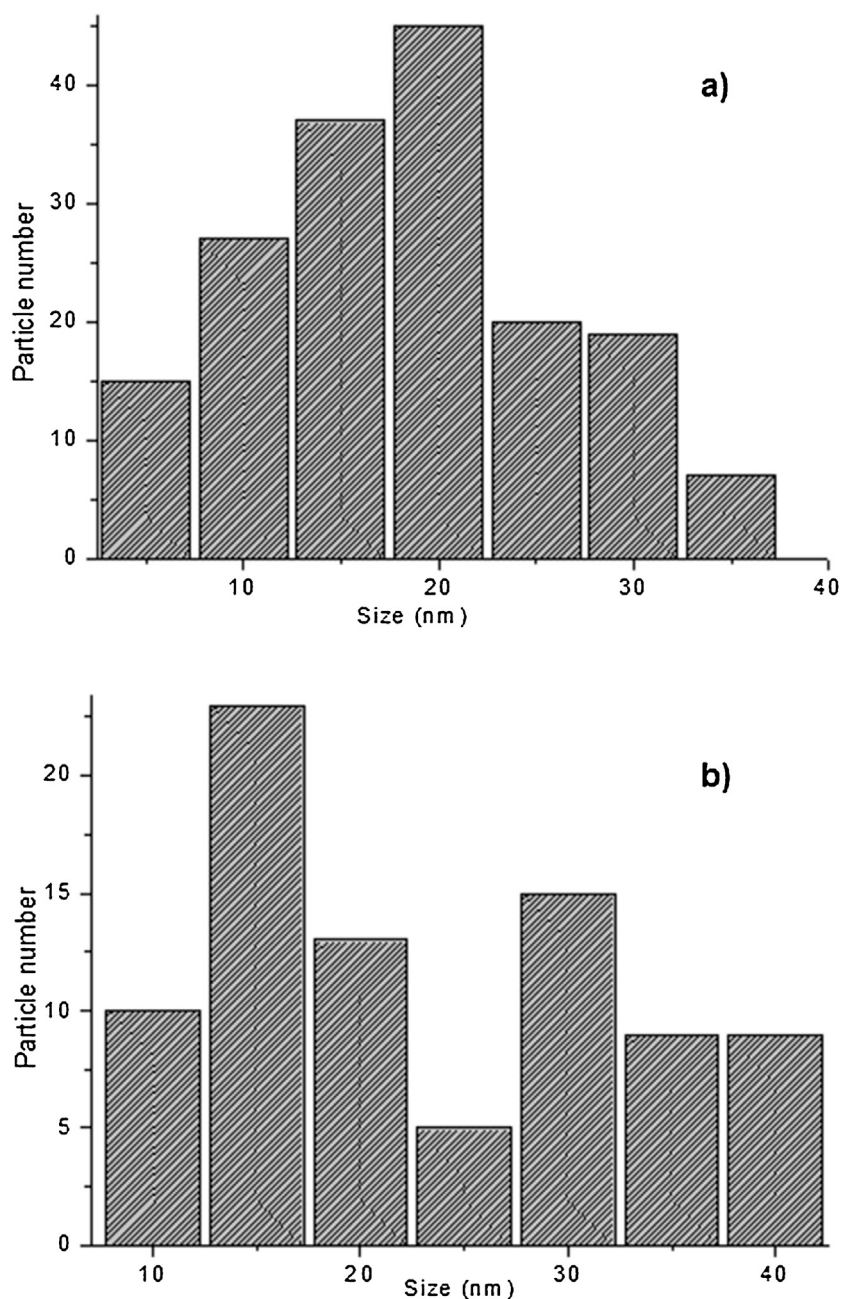

Fig. 1. XRD analysis of the TUF mineral and TUF/Fe-Cu nanocomposite.

Fig. 3. Distribution of sizes for spherical (a) and needle-shape (b) Fe-Cu nanostructures in the TUF/Fe-Cu nanocomposite.

presence of iron moieties in higher concentration in contrast with the copper. These results are confirming the proportion 75–25 wt.% of Fe-Cu employed to synthetized to obtain the composite. The mixture of both species also can suggest the formation of Fe-Cu oxides nanoparticles dispersed on the TUF/Fe-Cu nanocomposite in different proportions.

The nitrogen adsorption-desorption isotherm profile of the nanocomposite can be classified as type II isotherm and type H3 hysteresis loop according to BDDT classification [19]. This isotherm, and its hysteresis, is usually found on mesopore solids forming slit pores with nonuniform size. The plot of the pore size distribution from adsorption-desorption isotherm by BJH method confirms this idea, since the average pore diameter is 9.50 nm for

adsorption and 1.94 nm for desorption. The calculated BET surface area is 9.45 m^2/g.

The TUF/Fe-Cu nanocomposite has a pH$_{pzc}$ of 9.30. Same determination for TUF only yielded a value of 9.04. Therefore, accordingly to these results, it seems that the surface of the support material was modified due to the incorporation of the Fe-Cu oxides nanoparticles.

The composite has a rough and heterogeneous surface, with particles agglomerated of different shape and size, as can be observed in the SEM micrograph shown in Fig. 6a. The white points denoted by ellipse could be associated to metallic nanoparticles.

The micrograph after malachite green adsorption (TUF/Fe-Cu/MG) shows a smoother surface (Fig. 6b). In comparison with the
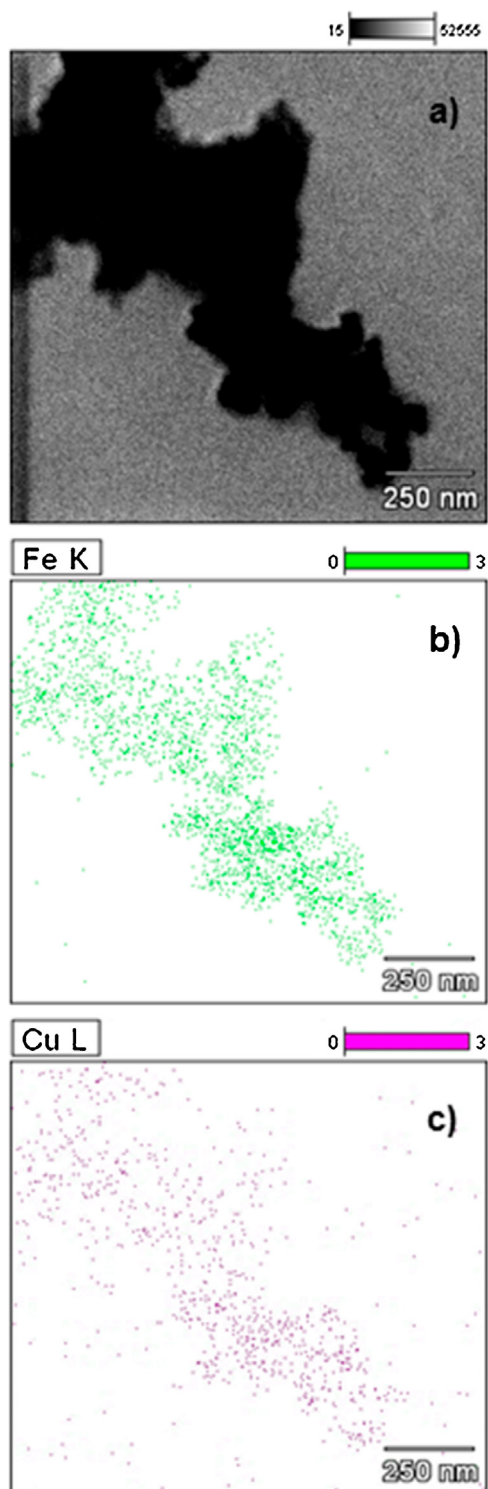
Fig. 4. EDS mapping of the TUF/Fe-Cu nanocomposite. STEM – Bright Field (BF) micrograph (a); Fe Kα signal (b); C) Cu Lα signal (c).

TUF/Fe-Cu nanocomposite micrographs, luminous points are not visible, which could be due to the interaction with dye molecules that can remain attached to the composite surface.

For the nanocomposite, the EDS analysis (Table 1, Fig. 6c) indicates a heterogeneous composition of alkaline, alkaline-earths and transition elements. In this case the major element is oxygen, followed by calcium, carbon, silicon, iron and copper. The biggest proportion of oxygen is due to the main phase of support material

(TUF), (calcite like $CaCO_3$) and the nanoparticles oxides, according to synthesis method selected in absence of inert atmosphere. The calcium, carbon and silicon are related to chemical composition of main phase in support material. The iron and copper are related with nanoparticles added to the support material.

IR spectra of TUF mineral, TUF/Fe-Cu nanocomposite and TUF/Fe-Cu/MG, are shown in Fig. 7. TUF exhibits main bands at 1500–700 cm^{-1} region. These bands evidence the presence of $CaCO_3$ [20], confirming the material's main phase. For the TUF/Fe-Cu nanocomposite, the appearance of new absorption bands about 1211.78 cm^{-1}, 1740.29 cm^{-1} and 2930–3010 cm^{-1} can be observed. Also, characteristic bands intensity of support material decrease and other disappear. All these confirm, to some extent, the chemical transformation of TUF material by the combination of surface groups with different chemical species of Fe and Cu that could be forming onto the nanostructures surface. When MG dye is adsorbed, the band intensities in the TUF/Fe-Cu nanocomposite decrease; in addition to the appearance of new bands in this spectrum, which corresponds to MG molecule, as observed in Fig. 7(b), confirms the removal of dye molecules by the TUF/Fe-Cu nanocomposite.

3.3. Adsorption kinetics

Adsorption kinetic is the relationship of adsorption capacity *versus* time; in this case, it refers to the quantification of the organic dye adsorbed in the adsorbent material from different contacting time. Fig. 8a shows the adsorption kinetic behavior for the Fe-Cu nanostructures and for the TUF/Fe-Cu nanocomposite. For the nanostructures alone, the equilibrium time was reached at 70 min, meanwhile for the composite the equilibrium time was reached at 160 min. This latest time is twice higher than TUF material (80 min) and nanostructures alone. It seems that the incorporation of nanoparticles in TUF interferes in the diffusion process, making the access to surface sites more difficult, which slows down the dye-adsorption process.

In order to elucidate the adsorption mechanism and potential rate controlling step of TUF/Fe-Cu nanocomposite, three kinetic models including the pseudo-first order, pseudo-second order, and intraparticle diffusion model [21] were used. These models give support information about occurrence and mechanism of adsorption on the composite. Values of correlation coefficient R^2 for the TUF/Fe-Cu nanocomposite were closer to one. The value of q_t experimental (q_{exp}) was closer to the value obtained for pseudo-first order model (q_{cal}). Therefore, the process was better described by pseudo-first order model (Table 2). It is, therefore, suggested that the removal of MG was carried by physisorption process, although we cannot rule out that chemical adsorption processes can occur simultaneously.

The dye adsorption process by composite particles occurs in several steps, this situation can be study using the intraparticle diffusion model. Since the intraparticle diffusion model does not satisfies the linear relationship with the experimental data, then the adsorption process may occur by two or more steps (Fig. 8b). In this case the plot gave three linear regions, attributed to the diffusion of dye molecule through the solution to the external surface of composite (I), to intraparticle diffusion with gradual equilibrium stage (II) and final equilibrium stage (III). In the graph, the plots are not linear over the whole time range, implying that more than one process is controlling the adsorption process [22]. Zones I and II can be identify as mesopores and micropores diffusion, respectively; also, zone I is similar in time range than II, indicating that the diffusion in mesopores is similar in extent to that in micropores diffusion. This agrees with the mesopores found in the composite, or mesopores close to micropores, which is confirmed by BET surface area obtained (*vide supra*).
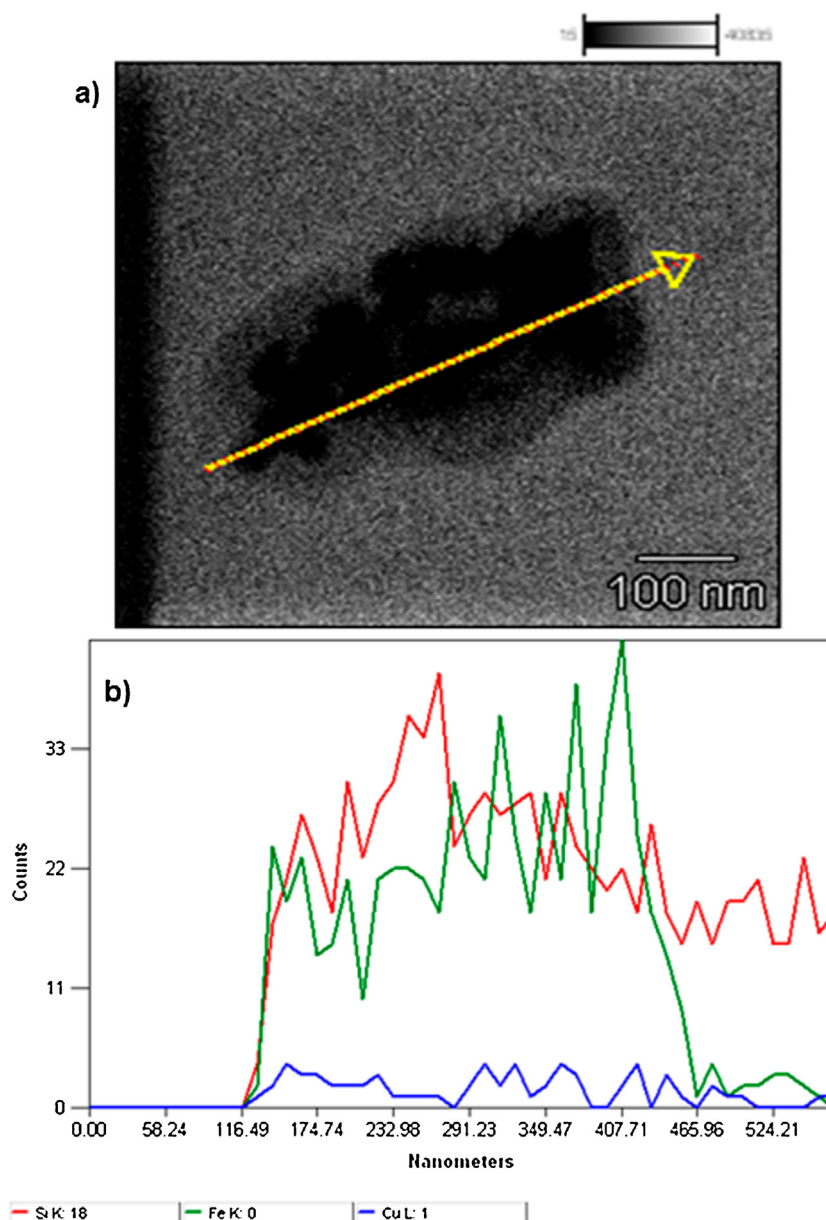
Fig. 5. STEM analysis of the TUF/Fe-Cu nanocomposite.

The results of applying kinetics models to natural material (TUF) and the TUF/Fe-Cu nanocomposite imply that incorporation of nanostructures did not modify the kinetic process. In addition, the kinetic rate constant was higher for TUF ($k_2 = 0.13$ g/mg min) than for the composite ($k_2 = 0.03$ g/mg min).

3.4. Effect of pH

pH of the aqueous solution plays an important role in the characteristics of adsorbate and the adsorbents efficiency [23]. The removal of MG dye by the TUF/Fe-Cu nanocomposite from aqueous solutions increases with pH of the solutions because there is an increase in the adsorption capacity (Fig. 9a). The Fig. 9b indicate that the adsorption of MG dye is weak in acidic conditions. It is posibly that the removal occur through electrostatic interaction at basic pH or a chemical reaction between the dye molecules and the TUF/Fe-Cu nanocomposite adsorbent.

One of the components of TUF is $CaCO_3$, in aqueous solution, carbonate ions (CO_3^{2-}) are present. Under low pH conditions, hydrogen ions (H^+) should interact with CO_3^{2-} to perhaps generate H_2CO_3, avoiding thus the interaction with MG molecules and decreasing the dye adsorption.

$$CO_3^{2-} + H^+ \rightleftarrows HCO_3^-$$

$$HCO_3^- + H^+ \rightleftarrows H_2CO_3$$
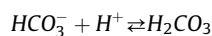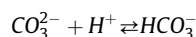
At a basic medium, with the presence of hydroxyl ions (OH^-), the interaction between CO_3^{2-} with OH^- is not possible, then the species present in aqueous solution could attract electrostatically the MG molecules promoting the removal of dye.
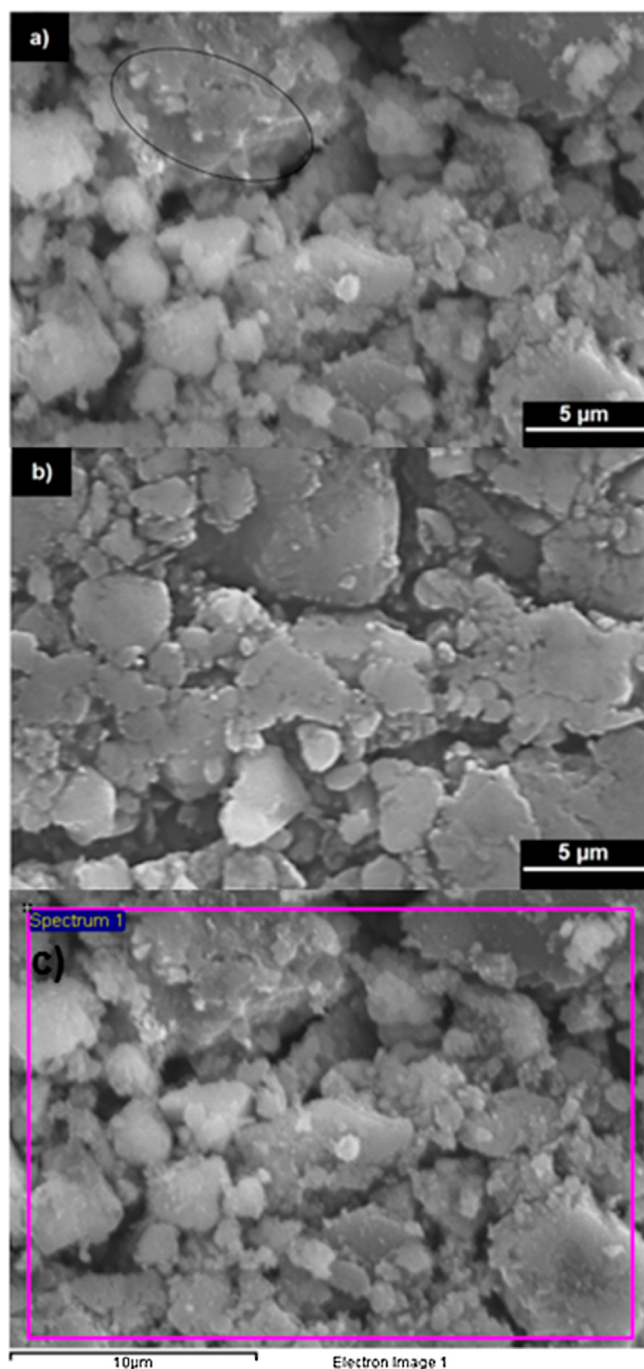
$$CO_3^{2-} + H_2O \rightleftarrows HCO_3^- + OH^-$$
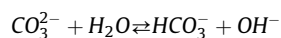
Fig. 6. SEM micrographs of TUF/Fe-Cu nanocomposite (a) and composite after malachite green dye adsorption (b; c), SEI, 20 kV, ×5000. (For interpretation of the references to colour in this figure legend, the reader is referred to the web version of this article.)

Besides, the transformation of MG molecule to MG-carbinol molecule under basic conditions is possible (Fig. 9b) and this can promote other processes of removal like electrostatic atraction, hydrogen bond interaction and/or chemical reaction.

3.5. Effect of temperature

The experimental results shown in Fig. 10 demonstrates that the adsorption capacity increases when the solution temperature also augments, which indicates that the adsorption of MG dye by the TUF/Fe-Cu nanocomposite is endothermic in nature.

The process is favored for higher temperatures perhaps due to a higher mobility of the dye molecules, accordingly to the increase of the rate constant of pseudo-second order model kinetics (k_2, Table 3) as well as of the diffusive movement.

The thermodynamic parameters were determined using Eqs. (3)–(6) (Table 4). The values of $\Delta H°$ (change in enthalpy, kJ/mol), $\Delta S°$ (change in entropy, kJ/molK) and E_a (energy of activation, kJ/mol) were obtained from slope and intercept of $\Delta G°$ vs. T and $\ln k_1$ vs. 1/T plot respectively [24].

$$K_c = \frac{C_a}{C_e} \tag{3}$$

$$\Delta G° = -RT \ln K_c \tag{4}$$

$$\Delta G° = \Delta H° - T\Delta S° \tag{5}$$

$$\ln k_1 = \ln A - \frac{E_a}{RT} \tag{6}$$

Where K_c is the equilibrium constant, C_e and C_a is the liquid and solid phase concentration at equilibrium (mg/L), T is the temperature (K), $\Delta G°$ is the change in free energy (kJ/mol) and R is the gas constant (8.31 J/mol).

Generally, the adsorption process is assigned to physisorption in nature when the $\Delta G°$ value is in the range of −20 to 0 kJ/mol, while values ranging from −400 to −80 kJ/mol suggests a chemisorption process [25]. The negative value of $\Delta G°$ for the intervals of solutions temperature confirms the spontaneous nature of adsorption and the adsorption efficiency of MG dye by the TUF/Fe-Cu nanocomposite with the increase in temperature. The endothermic nature of process is confirmed by the positive value of $\Delta H°$. Moreover, the enthalpy value for an adsorption process can also be used to distinguish between chemical and physical adsorption. For chemical adsorption, values of enthalpy change range from 83 to 830 kJ/mol, while for physical adsorption they range from 8 to 40 kJ/mol. Since this value is lower than 40 kJ/mol, this adsorption process can be considered as a physisorption process [26]. The value of E_a is between 5 and 40 kJ/mol (low values) thus, the adsorption is confirmed that occur through physisorption process [27]. The positive value of $\Delta S°$ show that the randomness increases at the solid-solution interface during the adsorption process of MG dye.

3.6. Effect of dye chemical structure

In order to study the adsorption capacity of the TUF/Fe-Cu nanocomposite against other organic dyes with evident chemical differences to MG dye, we decided to perform batch experiments with red congo (CR) and acid green 25 (AG25) dyes. The equilibrium time was different in all three cases. It is highest for MG adsorption, followed by CR and the lower for AG25 (Fig. 11a). The same behavior was observed for equilibrium time.

The composite removed greater amount of the cationic dye (MG) than anionic dyes (CR and AG25). The three structures are different regarding the number of functional groups, geometry and arrangement of molecules, and also the presence of acid (SO_3^-) and basic (CH_3N^-) groups (Fig. 11b–d). Probably the molecular size of the dyes influence the efficiency of the composite dye-adsorption capacity, because the TUF/Fe-Cu nanocomposite pores are narrow, then smaller compounds that should be better adsorbed tha larger ones. In addition, cationic dyes, such as MG, can be removed more easily using this composite because the cationic group may

Table 1
EDS analyses of TUF mineral, TUF/Fe-Cu nanocomposite and TUF/Fe-Cu/MG.

Elements	Weight percent (%)		
	TUF	TUF/Fe-Cu	TUF/Fe-Cu/MG
C	14.70 ± 11.72	8.69 ± 5.23	18.10 ± 6.41
O	48.46 ± 13.46	49.08 ± 6.69	48.71 ± 4.93
Na	0.01 ± 0.04	–	–
Mg	0.12 ± 0.10	0.11 ± 0.38	0.19 ± 0.31
Al	1.09 ± 1.06	0.87 ± 1.45	1.42 ± 0.64
Si	9.97 ± 8.51	5.80 ± 6.74	10.42 ± 10.20
Ca	25.18 ± 21.58	27.34 ± 11.75	15.36 ± 11.25
Fe	0.47 ± 0.46	5.74 ± 5.01	4.54 ± 2.03
K	–	0.53 ± 1.22	–
Ti	–	0.08 ± 0.26	–
Cu	–	1.76 ± 1.56	1.28 ± 1.12

interact electrostatically with surface groups of the nanocomposite, this also has concordance with the results of the kinetic analysis for MG dye.

3.7. Adsorption isotherms

The adsorption experimental data were fittted with Langmuir, Freundlich, Langmuir-Freundlich and Temkin adsorption models [28,29] (Table 5).

The best fit to experimental data was obtained with Langmuir-Freundlich model, which indicates the adsorption process occurs by combined mechanisms on a heterogeneous surface. The value of Freundlich parameter (1/n) was less than one, indicating a favorable adsorption [30].

Comparing the value of maximum adsorption capacity for the TUF/Fe-Cu nanocomposite (376.66 mg/g) to the value of TUF
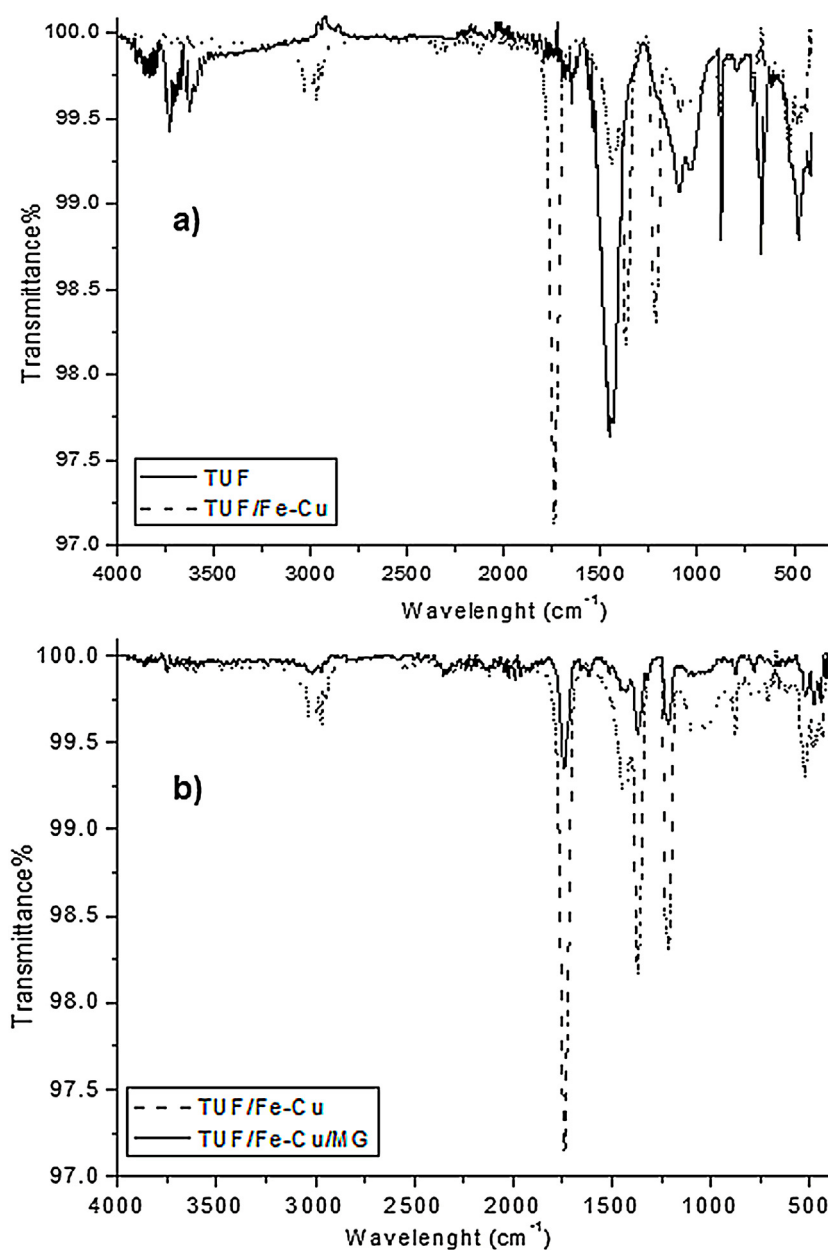

Fig. 7. FT-IR spectra of TUF (a), TUF/Fe-Cu nanocomposite (a; b) and TUF/Fe-Cu/MG (b).
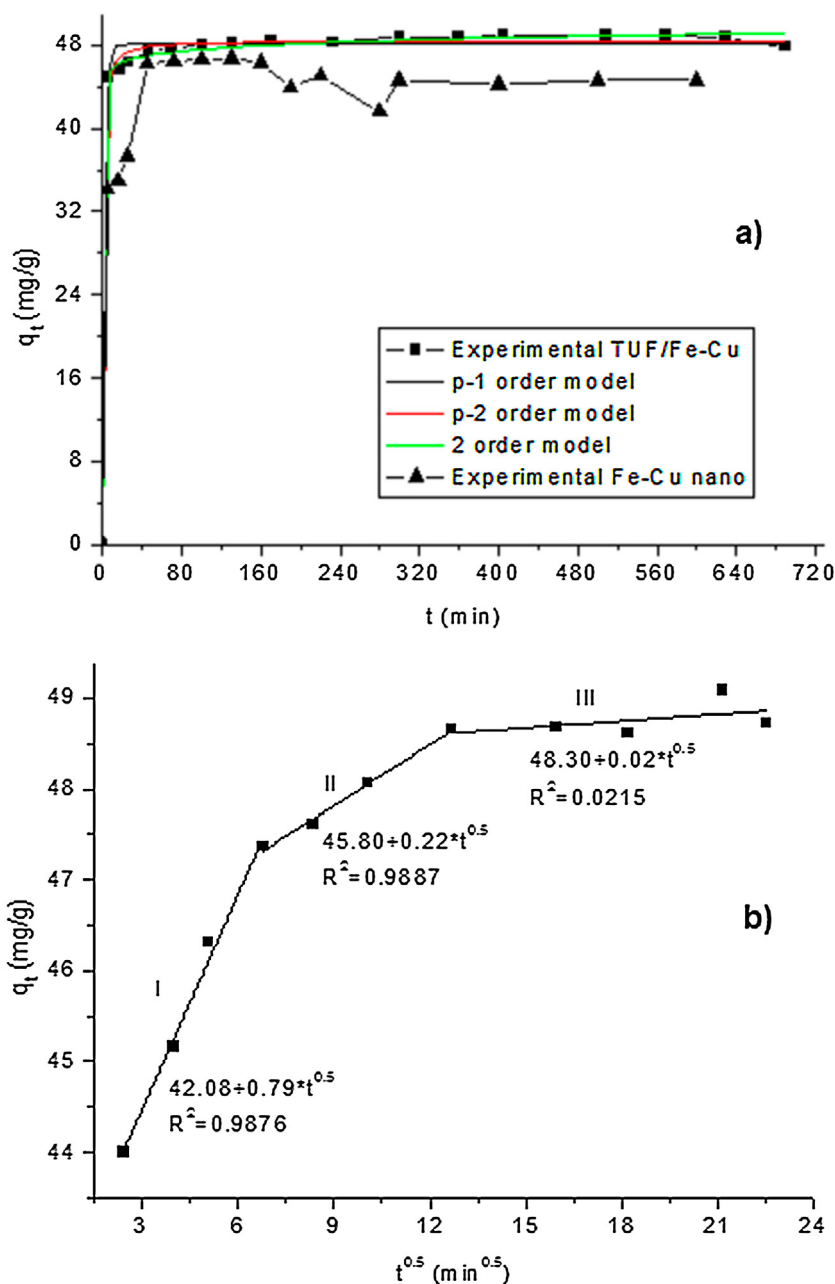
Fig. 8. Adsorption kinetics of nanostructures and TUF/Fe-Cu nanocomposite (a) and intraparticle diffusion plots for MG removal with the TUF/Fe-Cu nanocomposite (b).

Table 2
Kinetic parameters of the MG dye adsorption on TUF/Fe-Cu nanocomposite.

Parameters	TUF/Fe-Cu $q_{exp} = 48.00$ mg/g
Pseudo-first order model	
q_{cal} (mg/g)	47.84
k_1 (min^{-1})	0.42
R^2	0.9928
Pseudo-second order model	
q_{cal} (mg/g)	48.47
k_2 (g/mg min)	0.03
R^2	0.9979
Intraparticle diffusion model	
K_d (mg/g min$^{0.5}$)	0.22
R^2	0.9887

(212.75 mg/g), the former is almost twice higher than the latter. Therefore, the presence of nanostructures favored the removal process of MG dye. The use of Fe-Cu nanostructures supported on natural material or waste material has been reported for removal of azo dye [3]. However triphenylmethane dyes (MG) have not been studied that much with nanostructures adsorbents. The results obtained from this investigation prove the effective action of TUF/Fe-Cu nanocomposite for removal of basic dyes, such as malachite green. In fact, the adsorption capacity of 376.66 mg/g, is greater than the adsorption capacity in several systems studied for MG dye removal reported so far (Table 6).

Thus, under the same experimental conditions, the adsorption capacities of MG dye obtained for TUF, Fe-Cu nanostructures and the TUF/Fe-Cu nanocomposite are 212.75, 184.47 and 376.66 mg/g, respectively. Therefore, it seems that the presence of several
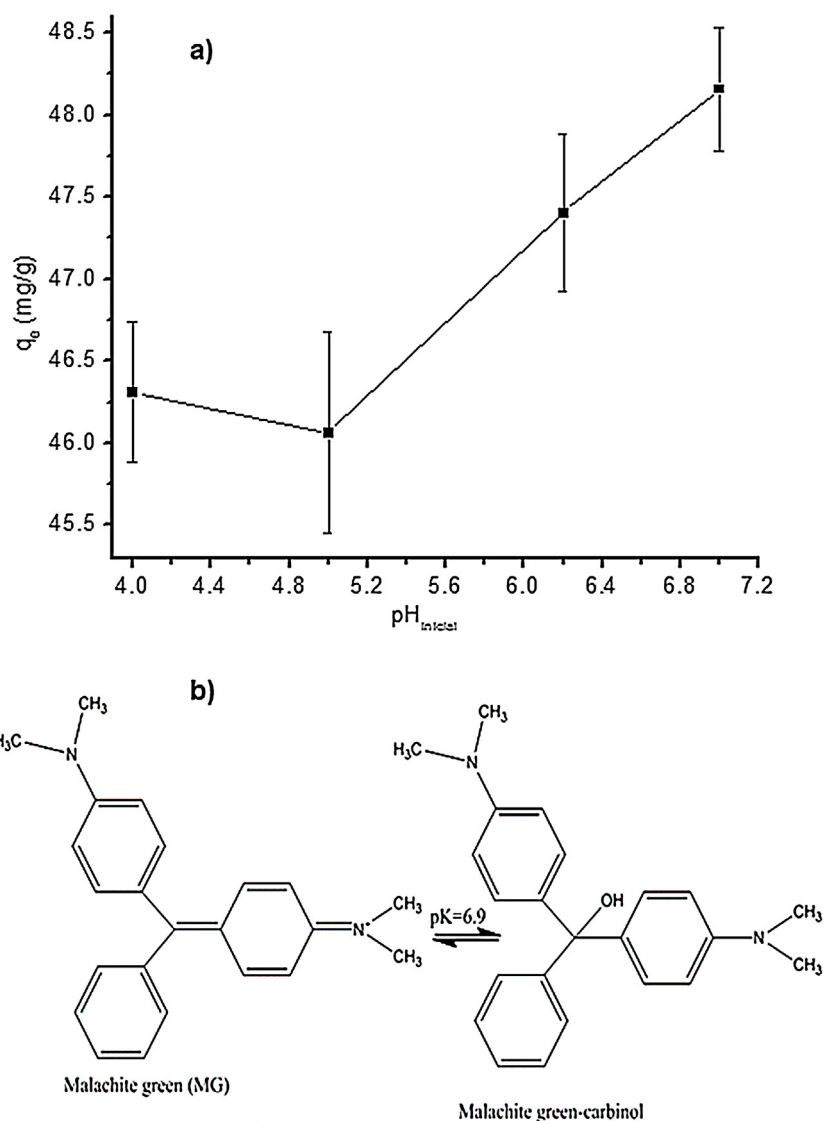
Fig. 9. Effect of pH on the adsorption of MG dye by the TUF/Fe-Cu nanocomposite: C_0=50 mg/L, m=10 mg, t_{eq} = 300 min, T = 298 K, stirring speed = 120 rpm (a) and equilibrium structures of MG related to pH (b).
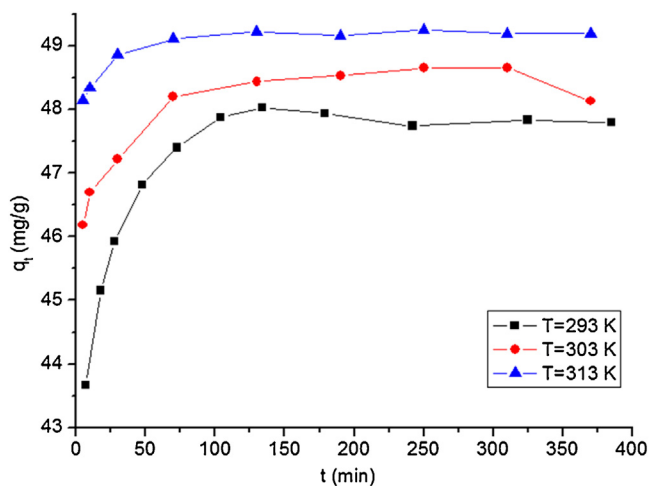

Fig. 10. Effect of temperature on the adsorption of MG dye by the TUF/Fe-Cu nanocomposite: C_0=50 mg/L, m=10 mg, T = 293, 303 y 313 K, stirring speed = 120 rpm.

phases in the mineral support, TUF, and the Fe-Cu oxides nanostructures embedded, generate synergic effects increasing the removal efficiency of MG dye with this novel composite and performing the dye removal through different processes, mainly physisorption.

Table 3
Kinetic parameters of the MG dye adsorbed on TUF/Fe-Cu nanocomposite at different temperatures.

Kinetic parameters	T=298 K	T=303 K	T=313 K
Pseudo-first order model			
q_{cal} (mg/g)	47.84	48.09	49.05
k_1 (min^{-1})	0.42	0.63	0.79
R^2	0.9928	0.9981	0.9997
Pseudo-second order model			
q_{cal} (mg/g)	48.47	48.38	49.19
k_2 (g/mg min)	0.03	0.08	0.16
R^2	0.9979	0.9994	0.9999

Table 4
Thermodynamic parameters for adsorption of MG dye on the TUF/Fe-Cu nanocomposite.

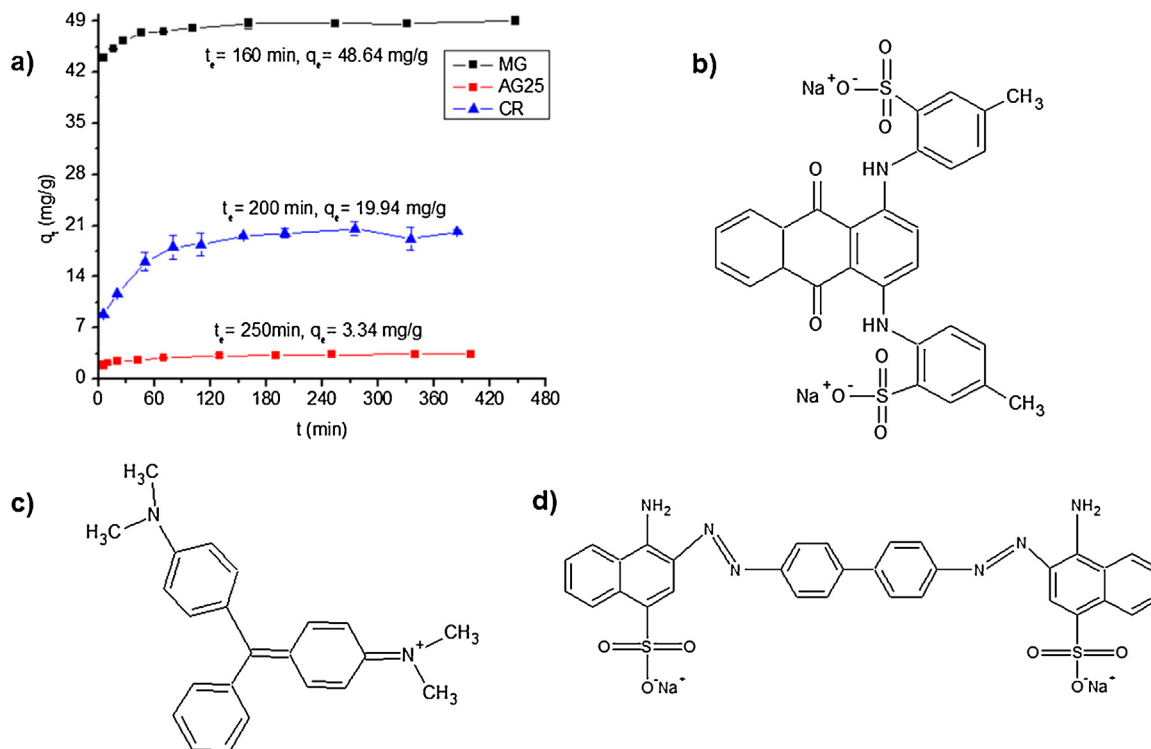| Temperature (K)	$\Delta G°$ (kJ/mol)	$\Delta H°$ (kJ/mol)	$\Delta S°$ (kJ/molK)	E_a (kJ/mol)	k_1 (min^{-1})
298	−7.78	36.23	0.15	29.41	0.42
303	−9.72				0.63
313	−10.79				0.79

Fig. 11. Effect of dye chemical structures in their removal by the TUF/Fe-Cu nanocomposite: C_0=50 mg/L, m=10 mg, T = 293 K, stirring speed = 120 rpm (a); chemical structures of AG25 (b), MG (c) and CR (d) dyes.

Table 5
Adsorption parameters of MG dye on TUF/Fe-Cu nanocomposite.

Langmuir		Freundlich		Langmuir-Freundlich		Temkin	
q_{max} (mg/g)	376.66	K_F (mg/g)(L/mg)$^{1/n}$	126.85	K (mg/g)	113.86	a (mg/g)	1.07
b (L/mg)	0.54	1/n	0.67	a (L/mg)^n	0.095	b(mg/g)	176.32
R^2	0.9830	R^2	0.9955	1/n	0.61	R^2	0.9940
				R^2	0.9954		

In addition, ICP-OES analysis indicated that 0.5 ppm of copper ion were desorbed. This allowed to infer that the amount of copper desorbed was fewer than the minimum value reported in the norm you referred [43].

4. Conclusion

Preparation of Fe-Cu nanostructures and novel TUF/Fe-Cu nanocomposite was achieved by a simple and inexpensive chemical reduction method. SEM, TEM, XRD and FT-IR results indicated the presence of Fe-Cu oxides nanoparticles supported or embedded on TUF material. The values of pH$_{zpc}$ compared to the value corresponding to TUF natural material showed the transformation of surface. TUF/Fe-Cu nanocomposite removed MG dye from aqueous solution in an efficent way. The adsorption kinetics of MG on this nanocomposite was better described by pseudo-first order model and, therefore, more than one process controlled the dye adsorption. The adsorption capacity was 376.66 mg/g, which is greater than the adsorption capacity in several systems studied for MG dye removal so far. The best removal conditions were basic pH and higher temperature. The nanocomposite exhibited more afinity for cationic and basic dye (MG) than anionic and acid dyes (CR and AG25). According to thermodynamic results, the adsorption method is better described by a physisorption process. The low cost and the ease synthetic methodology of this novel nanocomposite, as well as its high adsorption capacity of the MG organic dye, make this composite a potential large-scale efficient material to remove organic dyes and compounds.

Table 6
Adsorption capacity of MG dye by several adsorbents materials.

Adsorbents	Initial concentration (mg/L)	q_o (mg/g)	References
NiO nanoflakes	50	142.08	[31]
Sodium alginate-Fe_3O_4 nanoparticles	10–70	47.84	[32]
ZnO—NP-AC	5–30	322.58	[30]
AC from pine sawdust	–	370.37	
CAC Merck	–	222.22	
Oil palm trunk fiber	–	149.35	
Organically modified clay	10–500	40.48	[33]
ZnO—NP	10–40	310.50	[34]
SnO_2—NP		216.90	
Spent tea leaves	–	256	[35]
Cattail	–	196	
Tetraethylenepentamine-functionalized *Rosa canina*-L fruits activated carbon	–	333.3	[36]
Organically modified hydroxyapatite	–	188.18	[37]
Montmorillonite clay	–	262.49	[38]
carboxylate 2 functionalized multi-walled carbon nanotubes	50–200	49.45	[39]
Tamarix aphylla leaves	100–1000	303.03	[40]
Mesoporous aluminophosphate	100–500	24.51	[41]
Activated Carbon from Date Palm Leaf Wastes	–	47 mg/g	[42]
TUF	30–200	212.75	Previous work
TUF/Fe-Cu	30–200	376.66	This work

References

[1] P. Xu, G.M. Zeng, D.L. Huang, C.L. Feng, S. Hu, M.H. Zhao, C. Lai, Z. Wei, C. Huang, G.X. Xie, Z.F. Liux, Use of iron oxide nanomaterials in wastewater treatment: a review, Sci. Total Environ. (2012) 1–10.

[2] F. Zhang, X. Yin, W. Zhang, Development of magnetic $Sr_5(PO_4)_3(OH)/Fe_3O_4$ nanorod for adsorption of congo red from solution, J. Alloys Compd. 657 (2016) 809–817.

[3] J. Trujillo-Reyes, M. Solache-Ríos, A.R. Vilchis-Nestor, V. Sánchez-Mendieta, A. Colín-Cruz, Fe–Ni nanostructures and C/Fe–Ni composites as adsorbent for the removal of a textile dye from aqueous solution, Water Air Soil Pollut. 223 (2012) 1331–1341.

[4] T. Wang, J. Su, X. Jin, Z. Chen, M. Megharaj, R. Naidu, Functional clay supported bimetallic nZVI/Pd nanoparticles used for removal of methyl orange from aqueous solution, J. Hazard. Mater. 262 (2013) 819–825.

[5] G. López-Téllez, R.A. Morales-Luckie, O.F. Olea-Mejía, V. Sánchez-Mendieta, J. Trujillo-Reyes, V. Varela-Guerrero, A.R. Vilchis-Néstor, Nanoestructuras Metálicas: Síntesis, Caracterización Y Aplicaciones, first edition, Reverté, México, D.F, 2013.

[6] B.S. Kadua, Y.D. Sathea, A.B. Inglea, R.C. Chikatea, K.R. Patil, C.V. Rodec, Efficiency and recycling capability of montmorillonite supported Fe–Ni bimetallic nanocomposites towards hexavalent chromium remediation, Appl. Catal. B: Environ. 104 (2011) 407–414.

[7] F. Sadat, C. Falamaki, Zero valent nano-sized iron/clinoptilolite modified with zero valent copper for reductive nitrate removal, Process Saf. Environ. Protect. 91 (2012) 304–310.

[8] L. Yuhan, M. Long, P. Hu, Y. Chen, J. Huang, J. Hazard. Mater. 264 (2014) 195–202.

[9] A.R. Vilchis-Nestor, J. Trujillo-Reyes, J.A. Colín-Molina, V. Sánchez-Mendieta, M. Avalos-Borja, Biogenic silver nanoparticles on carbonaceous material from sewage sludge for degradation of methylene blue in aqueous solution, Int. J. Environ. Sci. Technol. 11 (2014) 977–986.

[10] M. Forbes, R. Vogwill, K. Onton, A characterisation of the coastal tufa deposits of south–west Western Australia, Sediment. Geol. 232 (2012) 52–65.

[11] C. Jiao, Y. Wang, M. Li, Q. Wu, C. Wang, Z. Wang, Synthesis of magnetic nanoporous carbon from metal-organic framework for the fast removal of organic dye from aqueous solution, J. Magn. Magn. Mater. 407 (2016) 24–30.

[12] L. Luo, C. Dai, A. Zhang, J. Wang, M. Liu, C. Song, X. Guo, A facile strategy for enhancing FeCu bimetallic promotion for catalytic phenol oxidation, Catal. Sci. Technol. 5 (2015) 3159–3165.

[13] J. Trujillo-Reyes, V. Sánchez-Mendieta, M.J. Solache-Ríos, A. Colín-Cruz, Obtención y caracterización de un composito de carbón activado y una nanoaleación de Fe/Cu como adsorbente, Rev. Latinoam. Rec. Nat. 4 (2008) 116–121.

[14] J. Trujillo-Reyes, V. Sánchez-Mendieta, A. Colín-Cruz, Removal of remazol yellow from aqueous solution using Fe–Cu and Fe–Ni nanoscale oxides and their carbonaceous composites, Environ. Technol. 33 (2012) 545–554.

[15] P. Faria, J. Órfão, M. Pereira, Adsorption of anionic and cationic dyes on activated carbons with different surface chemistries, Water Res. 38 (2004) 2043–2052.

[16] R.A. Morales-Luckie, Formación De Nanopartículas Fe-Cu: Su Caracterización Microestructural Y Determinación De Sus Propiedades Magnéticas. Tesis De Doctorado, Universidad Autónoma del Estado de México, Facultad de Química, Toluca, México, 2009.

[17] R.A. Morales-Luckie, V. Sanchez-Mendieta, J.A. Arenas-Alatorre, R. López-Castañares, J.L. Perez-Mazariego, V. Marquina-Fabrega, R. Wayne Gómez, One-step aqueous synthesis of stoichiometric Fe–Cu nanoalloy, Mater. Lett. 62 (2008) 4195–4197.

[18] A.D. Bokare, R.C. Chikate, C.V. Rode, K.M. Paknikar, Iron-nickel bimetallic nanoparticles for reductive degradation of azo dye Orange G in aqueous solution, Appl. Catal. B: Environ. 79 (2008) 270–278.

[19] M. Kruk, M. Jaroniec, K.P. Gadkaree, Nitrogen adsorption studies of novel synthetic active carbons, J. Colloid Interface Sci. 192 (1997) 250–256.

[20] N.V. Vagenas, A. Gatsouli, C.G. Kontoyannis, Quantitative analysis of synthetic calcium carbonate polymorphs using FT-IR spectroscopy, Talanta 59 (2003) 831–836.

[21] A. Blanco-Flores, A. Colín-Cruz, E. Gutiérrez-Segura, V. Sánchez-Mendieta, D.A. Solís-Casados, M.A. Garrudo-Guirado, R. Batista-González, Efficient removal of crystal violet dye from aqueous solutions by vitreous tuff mineral, Environ. Technol. 35 (2014) 1508–1519.

[22] V.S. Mane, P.V. Babu, Studies on the adsorption of Brilliant Green dye from aqueous solution onto low-cost NaOH treated saw dust, Desalination 273 (2011) 321–329.

[23] L. Hu, Z. Yang, L. Cui, Y. Li, H.H. Ngo, Y. Wang, Q. Wei, H. Ma, L. Yan, B. Du, Fabrication of hyperbranched polyamine functionalized graphene for high-efficiency removal of Pb(II) and methylene blue, Chem. Eng. J. 287 (2016) 545–556.

[24] D. Wang, L. Liu, X. Jiang, J. Yu, X. Chen, Desorption and removal of malachite green from aqueous solution using magnetic B-cyclodextrin-graphene oxide nanocomposites as adsorbents, Colloids Surf. A: Physicochem. Eng. Aspects 466 (2015) 166–173.

[25] P. Sharma, N. Hussain, D.J. Borah, M.R. Das, Kinetics and adsorption behavior of the methyl blue at the graphene oxide/reduced graphene oxide nanosheet_water interface: a comparative study, J. Chem. Eng. Data 58 (2013) 3477–3488.

[26] A.A. Jalil, S. Triwahyono, M.R. Yankob, Z.Z.A. Azmi, N. Sapawe, N.H.N. Kamaredin, H.D. Setiabudi, N.F. Jaafar, S.M. Sidik, S.H. Adam, B.H. Hameed, Utilization of bivale shell-treated Zea mays L. (maize) husk leaf as a low cost biosorbent for enhanced adsorption of malachite green, Bioresour. Technol. 120 (2012) 218–224.

[27] R.K. Gautam, V. Rawat, S. Banerjee, M.A. Sanroman, S.K. Singh, M.C. Chattopadhyaya, Synthesis of bimetallic Fe–Zn nanoparticles and its application towards adsorptive removal of carcinogenic dye malachite green and Congo red in water, J. Mol. Liq. 212 (2015) 227–236.

[28] A.M. Soliman, H.M. Elwy, T. Thiemann, Y. Majedi, F.T. Labata, N.A.F. Al-Rawashdeh, Removal of Pb(II) ions from aqueous solutions by sulphuric acid-treated palm tree leaves, J. Taiwan Inst. Chem. Eng. 58 (2016) 264–273.

[29] B. Mi-Hwa, I.C. Olakitan, O. Se-Jin, K. Dong-Su, Removal of Malachite Green from aqueous solution using degreased coffee bean, J. Hazard. Mater. 176 (2010) 820–828.

[30] M. Ghaedi, A. Ansari, M. Habibi, A. Asghari, Removal of malachite green from aqueous solution by zinc oxide nanoparticle loaded on activated carbon: kinetics and isotherm study, J. Ind. Eng. Chem. 20 (2014) 17–28.

[31] A.B. Wei, H. Liu, Y. Zhao, W. Chen, Y. Wang, H. Mab, S. Yang, Synthesis and formation mechanism of flowerlike architectures assembled from ultrathin NiO nanoflakes and their adsorption to malachite green and acid red in water, Chem. Eng. J. 239 (2014) 141–148.

[32] A. Mohammadi, H. Daemi, B. Mehdi, Fast removal of malachite green dye using novel superparamagnetic sodium alginate-coated Fe_3O_4 nanoparticles, Int. J. Biol. Macromol. 69 (2014) 447–455.

[33] S. Arellano-Cárdenas, S. López-Cortez, M. Cornejo-Mazón, J.C. Mares-Gutiérrez, Study of malachite green adsorption by organically modified clay using a batch method, Appl. Surf. Sci. 280 (2013) 74–78.

[34] K.Y. Kumar, H.B. Muralidhara, Y.A. Nayaka, J. Balasubramanyam, H. Hanumanthappa, Low-cost synthesis of metal oxide nanoparticles and their application inadsorption of commercial dye and heavy metal ion in aqueous solution, Powder Technol. 246 (2013) 125–136.

[35] H. Saygılı, F. Güzel, Performance of new mesoporous carbon sorbent prepared from grape industrial processing wastes for malachite green and congo red removal, Chem. Eng. Res. Des. 100 (2015) 27–38.

[36] M. Ghasemi, S. Mashhadi, M. Asif, I. Tyagi, S. Agarwal, V.K. Gupta, Microwave-assisted synthesis of tetraethylenepentamine functionalized activated carbon with high adsorption capacity for Malachite green dye, J. Mol. Liq. 213 (2016) 317–325.

[37] A.A. El-Zahhar, N.S. Awwad, Removal of malachite green dye from aqueous solutions using organically modified hydroxyapatite, J. Environ. Chem. Eng. 4 (2016) 633–638.

[38] B.A. Fil, Isotherm, kinetic, and thermodynamic studies on the adsorption behavior of malachite green dye onto montmorillonite clay, Part. Sci. Technol: Int. J. 34 (2016) 118–126.

[39] H. Sadegh, R. Shahryari-Ghoshekandi, S. Agarwal, I. Tyagi, M. Asif, V.K. Gupta, Microwave-assisted removal of malachite green by carboxylate functionalized multi-walled carbon nanotubes: kinetics and equilibrium study, J. Mol. Liq. 206 (2015) 151–158.

[40] M.A. Ackacha, M. Drmoon, Adsorption of malachite green dye onto novel adsorbent: *Tamarix aphylla* leaves, international conference on transport, Environ. Civil Eng. (2012) 141–145.

[41] C. Kannan, K. Muthuraja, M.R. Devi, Hazardous dyes removal from aqueous solution over mesoporous aluminophosphate with textural porosity by adsorption, J. Hazard. Mater. 244–245 (2013) 10–20.

[42] Y. Majedi, E. Alhilali, M. Al Nehayan, A. Rashed, S.S. Ali, N. al Rawashdeh, T. Thiemann, A. Soliman, Treatment of dye-loaded wastewater with activated carbon from date palm leaf wastes, The 4th World Sustainability Forum 2014 Glyph2Conference Proceedings Paper (2014). http://www.sciforum.net/conference/wsf-4.

[43] Norma de Calidad Ambiental y de Descarga de Efluentes: Recurso Agua (NCADE). LIBRO VI ANEXO 1, https://www.elaw.org/system/files/NCADE.doc.